MoS_2-on-paper optoelectronics: drawing photodetectors with van der Waals semiconductors beyond graphite

Ali Mazaheri[1,2], Riccardo Frisenda[1], Andres Castellanos-Gomez[1]*

[1]Materials Science Factory. Instituto de Ciencia de Materiales de Madrid (ICMM-CSIC), Madrid, E-28049, Spain.

[2]Nanophysics research Lab., Department of Physics. University of Tehran, Tehran 14395, Iran.

[*]andres.castellanos@csic.es

We fabricate paper-supported semiconducting devices by rubbing a layered molybdenum disulfide (MoS_2) crystal onto a piece of paper, similarly to the action of drawing/writing with a pencil on paper. We show that the abrasion between the MoS_2 crystal and the paper substrate efficiently exfoliates the crystals, breaking the weak van der Waals interlayer bonds and leading to the deposition of a film of interconnected MoS_2 platelets. Employing this simple method, that can be easily extended to other 2D materials, we fabricate MoS_2-on-paper broadband photodectectors with spectral sensitivity from the ultraviolet (UV) to the near-infrared (NIR). We also used these paper-based photodetectors to acquire pictures of objects by mounting the photodetectors in a homebuilt single-pixel camera setup.

Introduction

Handwriting and/or drawing on a piece of paper with a pencil has become a routine daily task for thousands of millions of people around the world due to their mass production that led to ubiquity and reduced cost. These common stationary items have recently jumped out of the writing/drawing realm and have been employed to fabricate electronic devices. This has been, most likely, motivated by the extremely low cost of paper substrates (paper ~0.1 €/m^2 as compared with PET ~2 €/m^2, PI ~30 €/m^2, crystalline silicon ~1000 €/m^2),[1,2] its biodegradability and its potential to allow the fabrication of flexible and even foldable electronic devices.[1,3–5]

The rough, fiber-based, structure of paper, however, is a handicap to fabricate devices using conventional lithographic techniques developed to fabricate devices on silicon wafers by the semiconductor industry. The use of graphite pencil lead traces, formed by the exfoliation of graphite platelets through the abrasion of the graphite lead while scribing on the paper substrate, allow to pattern electrically conductive pads on the rough surface of paper.[3,6,7] This simple approach has been used to demonstrate pencil-drawn-on-paper strain gauges, humidity, temperature, gas and chemical sensors.[6,8–15]

The lack of band gap in graphite, however, hampers the use of pencils to fabricate certain electronic devices, like digital electronics components or optoelectronics devices that require a

semiconductor material with a sizeable band gap. Nonetheless, the amount of works studying draw-on-paper semiconductor devices is still very scarce.[16–20]

Here we explore the potential of layered semiconducting materials to draw semiconductor devices through abrasion on paper. We select molybdenum disulfide (MoS_2) as an illustrative example of van der Waals semiconductor, which is abundant in nature in the mineral form of molybdenite. We demonstrate that the layered structure of MoS_2, very similar to that of graphite, allows for drawing MoS_2 platelets traces on paper by simply rubbing a MoS_2 crystal against a paper substrate. We show the potential of the fabricated devices as broadband photodectectors with spectral sensitivity in the ultraviolet (UV), visible (VIS) and near-infrared (NIR) range. Moreover, the paper-based photodetectors can be used to acquire pictures of objects by integrating these photodetectors in a single-pixel camera setup. The fabrication process described here is a general one and could be straightforwardly applied to other van der Waals semiconductors opening a wide field of research.

Results and discussion

Paper-supported device fabrication

The device fabrication starts by printing the electrodes outline with a laser printer (Brother MFC-L5700DN) on conventional Xerox paper (80 gr/m^2), see Figure 1.1. The semiconductor channel area is delimited by using scotch tape (3M, MagicTape®) to make a square mask. A freshly cleaved molybdenite crystal (Wolfram Camp mine, Queensland, Australia) is rubbed against the unmasked paper to form a homogeneous coverage, see Figure 1.2. In order to improve the homogeneity of the MoS_2 film we blur the as-drawn MoS_2 film with a cotton swab, Figure 1.3. We repeat the MoS_2 rub + blur steps 4 times until obtaining a highly homogeneous MoS_2 film, see Figure 1.4. We then remove the tape mask and we fabricate graphite electrodes by drawing with a 4B pencil (with an approximate composition of ~80% graphite, ~15% clay, ~5% wax)[21] filling the printed outline, Figure 1.5. Interestingly, this shows that it is possible to 'draw' different van der Waals materials on top of each other to build multi-layered structures with dissimilar 2D materials. This can be of interest for the fabrication of vertical devices or other electronic components. Figure 1.6 shows an optical picture of a finished devices. In order to solder wires, two pieces of electrically conductive copper tape are adhered on top of the graphite pads. We find that the contact between the graphite electrodes and the MoS_2 channel is Ohmic with a contact resistance of ~20 MΩ (see the Supporting Information for details about the contact resistance measurement through a transfer length method). We also determine the sheet resistance of our devices that ranges from ~0.5-10 GΩ/sq. Considering an average MoS_2 film thickness of 5-15 µm[21] we estimate that the conductivity of the drawn MoS_2 on paper films is in the $5\cdot10^{-6}$-$1.5\cdot10^{-4}$ S/m range. Interestingly, this conductivity range is higher than that reported for networks of liquid phase exfoliated MoS_2 ($6\cdot10^{-7}$ - $2.5\cdot10^{-6}$ S/m),[22,23] most likely due to the

presence of solvent residues at the interfaces of liquid exfoliated materials that can impair the electrical conductivity.

Optoelectronic characterization

The performance of the fabricated MoS_2-on-paper devices as photodetectors is studied by measuring their electrical transport characteristics with a source measurement unit (Keithley 2450) in dark and upon illumination. We use high-power fiber-coupled LED sources (Thorlabs) with 18 different wavelengths to study the spectral response. A spot of 67 mm^2 in area with a power of 30 mW is used for all the photocurrent measurements at different wavelengths. Figure 2a shows the current *vs*. voltage curve (*IV* hereafter) acquired for the device in the dark state and upon illumination with selected wavelengths showing a clear photoresponse. To verify if the MoS_2 channel is the main source of the photogenerated current we show in the Supporting Information the measurement on a graphite-on-paper device with a poor response to illumination. Figure 2b shows the current flowing through the device as a function of time when the illumination is switched ON and OFF to determine the response speed of the devices. When the illumination is switched ON, the photodetector shows an initial sharp response (faster than 0.2 s) followed by a slower response (~20-30 s) which indicates a superposition of different photocurrent mechanisms. The sharp response is typically observed in devices whose photocurrent generation is dominated by the photoconductive effect. Other photogeneration mechanisms like photogating or bolometric could be the source of the observed slow response.[24–28] The photocurrent can be determined by subtracting the dark current to the current under illumination. The responsivity, a common figure-of-merit that allows the comparison between different photodetectors, can be calculated as:

$$R = \frac{I_{ph}}{P} \cdot \frac{A_{spot}}{A_{sample}}$$

Where I_{ph} is the photocurrent, P is the effective power, A_{spot} is the area of the focused spot and A_{spot} is the illuminated active area of the device. Figure 2c summarizes the responsivity of the device at different illumination wavelength in the 365 nm to 940 nm range. Interestingly, the MoS_2-on-paper photodetector shows a very broad spectral response with a shallow peak at 550-750 nm that matches the spectral range where the optical absorption of multilayer MoS_2 gets enhanced due to the presence of the A and B excitonic resonances.[29,30] Although there are some reports about photoresponse in multilayer MoS_2 detectors working in the NIR, the typical response drops abruptly beyond 670 nm.[31,32] This extended spectral response also suggest the presence of other photogeneration mechanism like bolometric effect.

The responsivity reaches a value of ~1.5 μA/W, much smaller than that of MoS_2 nanodevices based on single crystals.[26,33,34] This reduced performance is expected for a macroscopic device formed by the overlap of small crystallites as a higher density of recombination centers is

expected. Nonetheless, the responsivity value is comparable to that of devices based on liquid phase exfoliation or inkjet printing.[35,36] Note that operating the photodetector at higher temperatures the responsivity can be increased up to 10 µA/W (see the Supporting Information). In order to get a deeper insight about the physical mechanism behind the photocurrent generation we studied the power and bias voltage dependence of the photocurrent. Figure 3a shows the current flowing in the devices as function of time while the illumination is switched ON and OFF for different incident powers (going from 5 mW to 75 mW). Figure 3b displays the generated photocurrent as a function of the power density that shows a marked linear relationship. The responsivity is thus almost independent on the power density (Figure 3c). Figure 3d and 3e show similar measurements to 3a and 3b respectively but varying the bias voltage instead of the power density. The photocurrent is linearly proportional to the bias voltage that yields increasingly high responsivity for higher voltages. (Figure 3f). The linear power and bias dependence of the photocurrent points to a major contribution of the photoconductive effect, which would explain the initial sharp response of our devices to modulated light. The linear power dependence also rules out completely the photogating effect as the source of the slow response component of the photogenerated current. In fact, photogating is characterized by a sublinear power dependence.[24–28] The bolometric effect, on the other hand, would be compatible with a linear power and bias dependence of the photocurrent and thus it could be the origin of the slow response component. Moreover, the bolometric effect would explain the broadband spectral response. In this scenario, the graphite electrodes would absorb light in a broad spectral range (even beyond that of MoS_2) increasing the temperature of the device, thus changing its resistance. In support to this scenario, in the Supporting Information we show how the MoS_2 device has a strong temperature dependent resistance.

Paper-based single-pixel camera imaging device

To further demonstrate the potential of these photodetectors, we mount them in a homebuilt single-pixel camera setup to image objects. The linear response to light of these paper-based photodetectors makes them as ideal active elements in imaging. Figure 4a is a sketch of the experimental setup. Briefly the object to be imaged is mounted on a motorized XY stage (Standa, 2x 8MT167S-25LS stages with 8SMC5-USB-B9-2 controller). A reflection-probe fiber bundle (RP29, Thorlabs) is used to illuminate and to probe the light reflected by the object under study (sample). This reflection-probe fiber bundle is bifurcated with three legs: one leg pointing towards the sample (sample leg), one leg carries light from a source towards the sample (light source leg) and another leg carries the light reflected by the sample to the photodetector (photodetector leg). By raster-scanning the object in the X and Y directions, one can construct a map of photocurrent that is linearly proportional to the reflectivity change in the object. Figure

4b compares the picture of a paper smiley acquired with a cell phone camera and a photocurrent map acquired with the MoS_2-on-paper photodetector single-pixel camera.

Conclusions

In summary, we have demonstrated how van der Waals materials beyond graphite can be used to draw devices on paper. In particular, we show how the layered structure of MoS_2 allows to deposit interconnected platelet traces on the surface of paper by simply rubbing a MoS_2 crystal against a piece of common paper. We also show how this simple method can be used to fabricate MoS_2-on-paper photodetectors with a remarkable broad spectral range. We have characterized the performance of these photodetectors finding that the photocurrent is generated by a superposition of photoconductive and bolometric effects, with responsivity values in the order of 1-2 μA/W (and even up to 10 μA/W when the device is operated at 70 ºC). Finally, we successfully demonstrate the potential use of these paper-based photodetectors by integrating one on a single-pixel camera setup to acquire images of objects.

Acknowledgements

This project has received funding from the European Research Council (ERC) under the European Union's Horizon 2020 research and innovation programme (grant agreement n° 755655, ERC-StG 2017 project 2D-TOPSENSE). R.F. acknowledges the support from the Spanish Ministry of Economy, Industry and Competitiveness through a Juan de la Cierva-formación fellowship 2017 FJCI-2017-32919. We acknowledge support of the publication fee by the CSIC Open Access Publication Support Initiative through its Unit of Information Resources for Research (URICI).

Notes and references

‡ During the elaboration of this manuscript we became aware of the pre-print by Nutting *et al*. [37] where the authors report the fabrication of paper-supported electronic devices based on different layered materials by means of abrasion of fine powder of the layered material against paper.

1 D. Tobjörk and R. Österbacka, *Adv. Mater.*, 2011, **23**, 1935–1961.
2 A. Russo, B. Y. Ahn, J. J. Adams, E. B. Duoss, J. T. Bernhard and J. A. Lewis, *Adv. Mater.*, 2011, **23**, 3426–3430.
3 N. Kurra and G. U. Kulkarni, *Lab Chip*, 2013, **13**, 2866–2873.
4 G. Zheng, Y. Cui, E. Karabulut, L. Wågberg, H. Zhu and L. Hu, *MRS Bull.*, 2013, **38**, 320–325.
5 C. Casiraghi, M. Macucci, K. Parvez, R. Worsley, Y. Shin, F. Bronte, C. Borri, M. Paggi and G. Fiori, *Carbon N. Y.*, 2018, **129**, 462–467.
6 N. Kurra, D. Dutta and G. U. Kulkarni, *Phys. Chem. Chem. Phys.*, 2013, **15**, 8367–8372.
7 V. V Brus and P. D. Maryanchuk, *Carbon N. Y.*, 2014, **78**, 613–616.
8 C.-W. Lin, Z. Zhao, J. Kim and J. Huang, *Sci. Rep.*, 2014, **4**, 3812.
9 N. Dossi, R. Toniolo, A. Pizzariello, F. Impellizzieri, E. Piccin and G. Bontempelli, *Electrophoresis*, 2013, **34**, 2085–2091.
10 T. Dinh, H.-P. Phan, D. V. Dao, P. Woodfield, A. Qamar and N.-T. Nguyen, *J. Mater. Chem. C*, 2015, **3**, 8776–8779.

11 T.-K. Kang, *Appl. Phys. Lett.*, 2014, **104**, 73117.
12 Y. Zhang, Z. Duan, H. Zou and M. Ma, *Sensors Actuators B Chem.*, 2018, **261**, 345–353.
13 S. Kanaparthi and S. Badhulika, *Green Chem.*, 2016, **18**, 3640–3646.
14 K. A. Mirica, J. G. Weis, J. M. Schnorr, B. Esser and T. M. Swager, *Angew. Chemie Int. Ed.*, 2012, **51**, 10740–10745.
15 Z. Zhu, H. Zhang, K. Xia and Z. Xu, *Microsyst. Technol.*, 2018, **24**, 3499–3502.
16 V. V Brus, M. Gluba, J. Rappich, F. Lang, P. D. Maryanchuk and N. H. Nickel, *ACS Appl. Mater. Interfaces*, 2018, **10**, 4737–4742.
17 V. V Brus, P. D. Maryanchuk, Z. D. Kovalyuk and S. L. Abashyn, *Nanotechnology*, 2015, **26**, 255501.
18 S. Liu, Z. Huang, H. Qiao, R. Hu, Q. Ma, K. Huang, H. Li and X. Qi, *Nanoscale Adv.*
19 F. Cao, D. Yu, X. Li, Y. Zhu, Z. Sun, Y. Shen, Y. Wu, Y. Wei and H. Zeng, *J. Mater. Chem. C*, 2017, **5**, 7441–7445.
20 Y. Zhang, L. Ge, M. Li, M. Yan, S. Ge, J. Yu, X. Song and B. Cao, *Chem. Commun.*, 2014, **50**, 1417–1419.
21 M. C. Sousa and J. W. Buchanan, in *Computer Graphics Forum*, Wiley Online Library, 2000, vol. 19, pp. 27–49.
22 D. J. Finn, M. Lotya, G. Cunningham, R. J. Smith, D. McCloskey, J. F. Donegan and J. N. Coleman, *J. Mater. Chem. C*, 2014, **2**, 925–932.
23 G. Cunningham, M. Lotya, N. McEvoy, G. S. Duesberg, P. van der Schoot and J. N. Coleman, *Nanoscale*, 2012, **4**, 6260–6264.
24 M. Buscema, J. O. J. O. Island, D. J. D. J. Groenendijk, S. I. S. I. Blanter, G. A. G. A. Steele, H. S. J. H. S. J. van der Zant and A. Castellanos-Gomez, *Chem. Soc. Rev.*, 2015, **44**, 3691–3718.
25 J. O. Island, S. I. Blanter, M. Buscema, H. S. J. Van Der Zant and A. Castellanos-Gomez, *Nano Lett.*, , DOI:10.1021/acs.nanolett.5b02523.
26 D. Kufer and G. Konstantatos, *Nano Lett.*, 2015, **15**, 7307–7313.
27 M. M. Furchi, D. K. Polyushkin, A. Pospischil and T. Mueller, *Nano Lett.*, 2014, **14**, 6165–70.
28 C. C. Wu, D. Jariwala, V. K. Sangwan, T. J. Marks, M. C. Hersam and L. J. Lauhon, *J. Phys. Chem. Lett.*, 2013, **4**, 2508–2513.
29 A. Castellanos-Gomez, J. Quereda, H. P. Van Der Meulen, N. Agraït and G. Rubio-Bollinger, *Nanotechnology*, , DOI:10.1088/0957-4484/27/11/115705.
30 Y. Niu, S. Gonzalez-Abad, R. Frisenda, P. Marauhn, M. Drüppel, P. Gant, R. Schmidt, N. Taghavi, D. Barcons, A. Molina-Mendoza, S. de Vasconcellos, R. Bratschitsch, D. Perez De Lara, M. Rohlfing and A. Castellanos-Gomez, *Nanomaterials*, 2018, **8**, 725.
31 W. Choi, M. Y. Cho, A. Konar, J. H. Lee, G.-B. Cha, S. C. Hong, S. Kim, J. Kim, D. Jena, J. Joo and S. Kim, *Adv. Mater.*, 2012, **24**, 5832–6.
32 J. Wu, Y. T. Chun, S. Li, T. Zhang, J. Wang, P. K. Shrestha and D. Chu, *Adv. Mater.*, 2018, **30**, 1705880.
33 O. Lopez-Sanchez, D. Lembke, M. Kayci, A. Radenovic and A. Kis, *Nat. Nanotechnol.*, 2013, **8**, 497–501.
34 Z. Yin, H. Li, H. Li, L. Jiang, Y. Shi, Y. Sun, G. Lu, Q. Zhang, X. Chen and H. Zhang, *ACS Nano*, 2012, **6**, 74–80.
35 S. Ghosh, A. Winchester, B. Muchharla, M. Wasala, S. Feng, A. L. Elias, M. B. M. Krishna, T. Harada, C. Chin and K. Dani, *Sci. Rep.*, 2015, **5**, 11272.
36 D. McManus, A. Dal Santo, P. B. Selvasundaram, R. Krupke, A. LiBassi and C. Casiraghi, *Flex. Print. Electron.*, 2018, **3**, 34005.
37 D. Nutting, J. F. Felix, S. Dong-Wook, A. De Sanctis, M. F. Craciun, S. Russo, H. Chang, N. Cole, A. Woodgate and I. Leontis, *arXiv Prepr. arXiv1911.12843*.

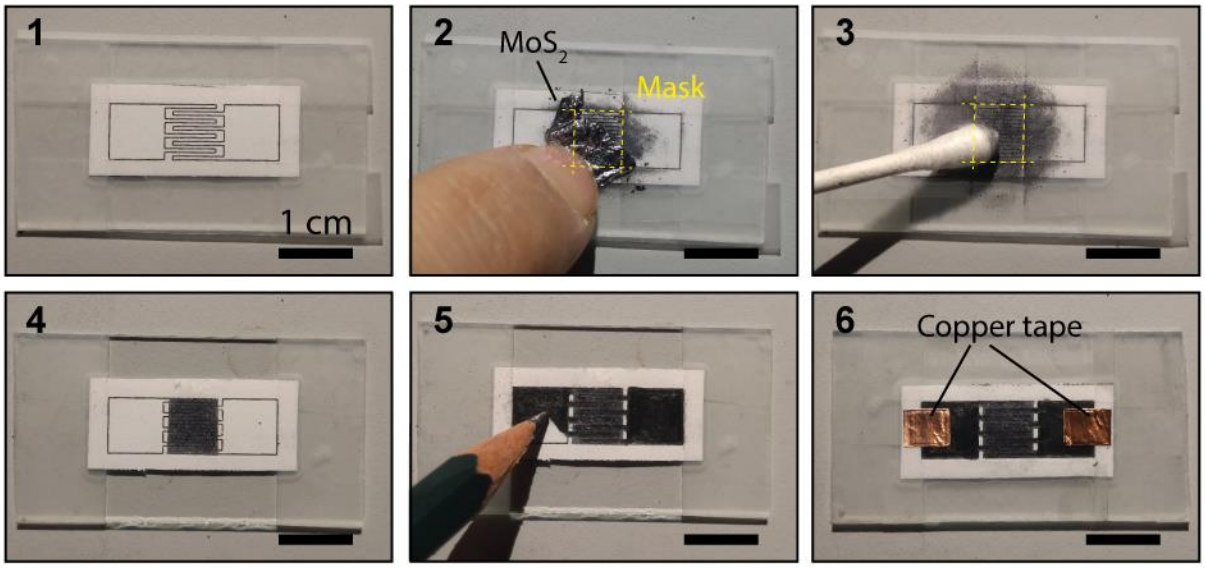

Figure 1. Pictures of the fabrication process of a MoS_2-on-paper photodetector. (1) The outline of the interdigitated electrodes is printed out in an office laser printer, the paper is cut and fixed onto a glass slide with adhesive tape. (2) A square mask is made in the device active area with adhesive tape and a MoS_2 crystal is rubbed against the bare paper area. (3) The drawn-MoS_2 is blurred with a cotton swab to improve the homogeneity. (4) After repeating the rubbing + blurring steps 4 times the mask is removed yielding to a very homogeneous MoS_2 square film. (5) The electrodes are drawn, following the printed outline, with a 4B pencil. (6) Two squares of copper tape are adhered to the graphite pads to allow soldering wires.

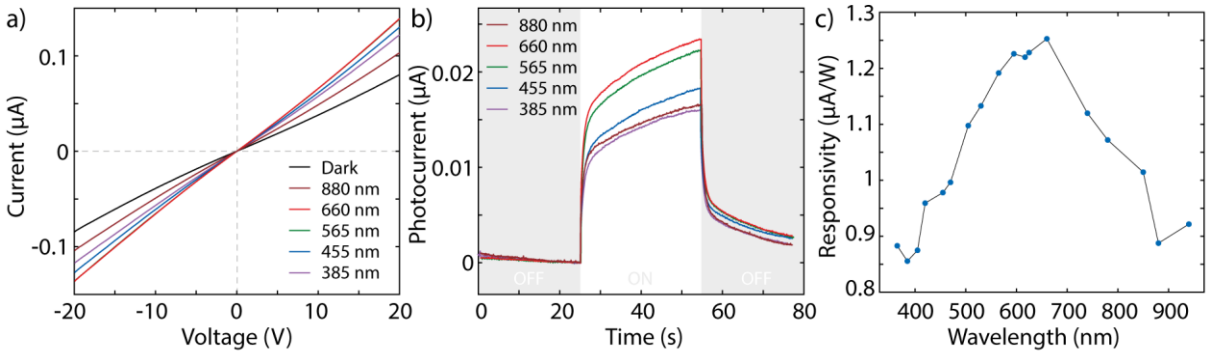

Figure 2. Optoelectronic response of the as-drawn MoS_2 photodetectors. (a) Current *vs.* voltage characteristics of the MoS_2-on-paper device in dark and upon illumination with selected illumination wavelengths (incident power 30 mW). (b) Photocurrent (current minus dark current value) flowing across the device (at a fixed bias voltage) as a function of time while the illumination with selected wavelengths is switched ON and OFF. (c) Responsivity spectrum of the device in the visible and near-infrared. Note: (b) and (c) measurements are carried out at V_{bias} = 20 V and incident power of 30 mW.

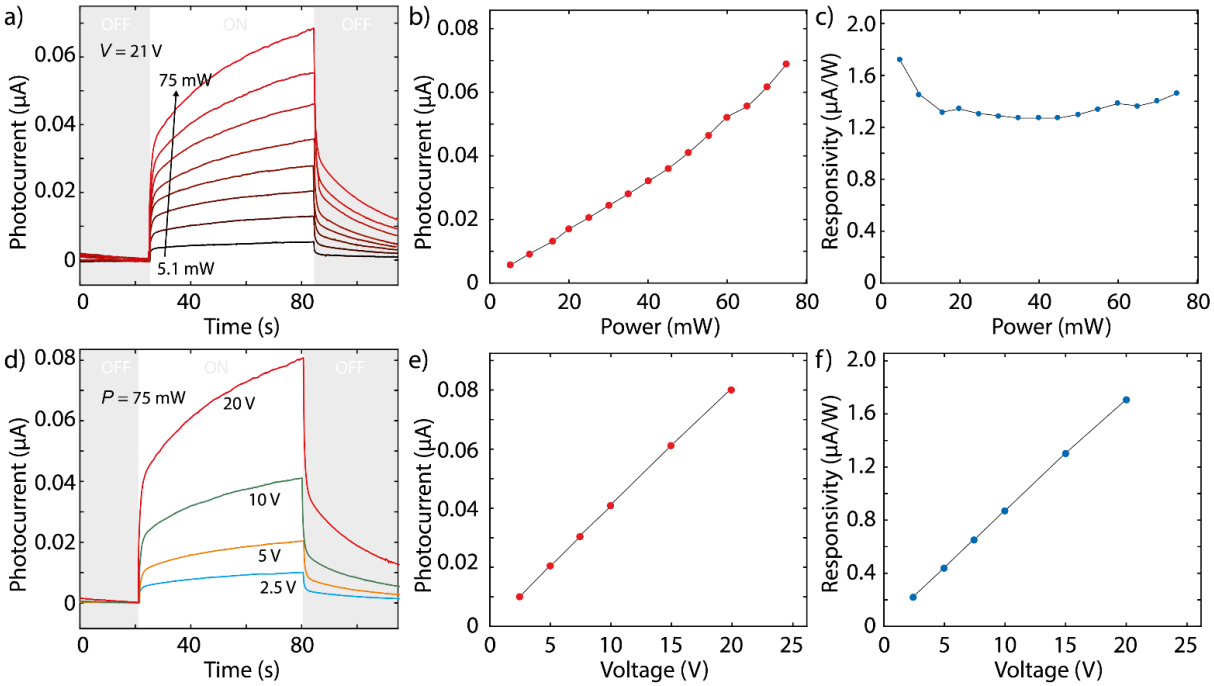

Figure 3. Power and bias dependence of the photocurrent generation in the as-drawn MoS_2 photodetectors. (a) and (b) Power dependence of the photocurrent (at a fixed bias voltage V = 21 V). (c) Responsivity as a function of the incident power showing a rather constant value around 1.4 μA/W. (d) and (e) Bias voltage dependence of the generated photocurrent. (f) Bias voltage dependence of the responsivity of the device (at a fixed wavelength of 660 nm and fixed power of 75 mW).

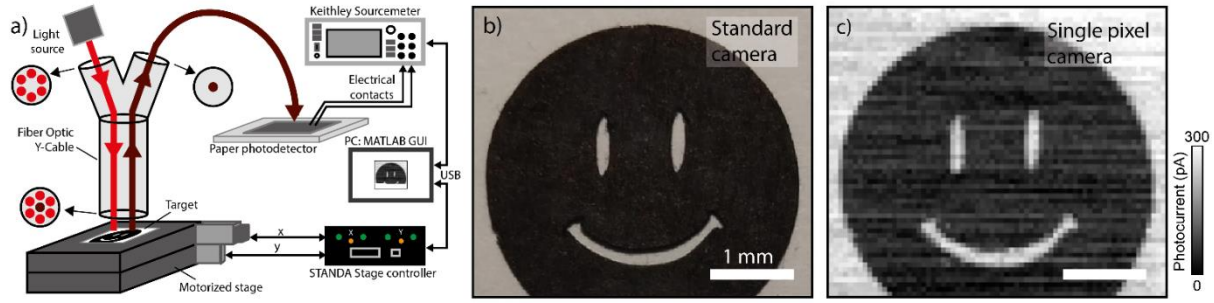

Figure 4. Integration of the MoS_2-on-paper photodetector in a single-pixel camera system to acquire images. (a) Schematic diagram of the experimental setup. (b) Image of the object under study acquires with a standard camera. (c) Image of the same object acquired with the single-pixel camera system based on a MoS_2-on-paper photodetector.

Supporting Information:

MoS_2-on-paper optoelectronics: drawing photodetectors with van der Waals semiconductors beyond graphite

Ali Mazaheri[1,2], Riccardo Frisenda[1], Andres Castellanos-Gomez[1]*

[1]Materials Science Factory. Instituto de Ciencia de Materiales de Madrid (ICMM-CSIC), Madrid, E-28049, Spain.

[2]Nanophysics research Lab., Department of Physics. University of Tehran, Tehran 14395, Iran.

[*]andres.castellanos@csic.es

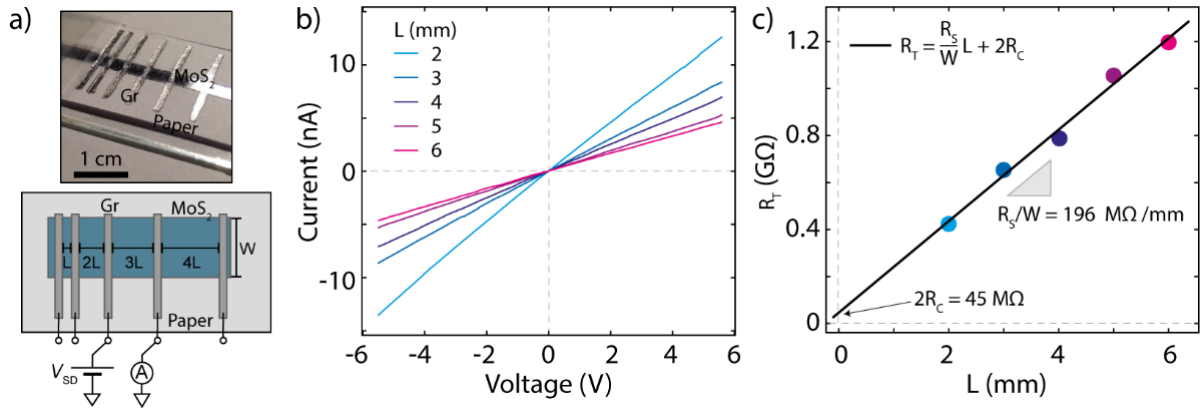

Figure S1. Contact resistance measurement though the transfer length method. (a) picture and scheme of the fabricated device. The width (W) of the MoS_2 strip is 2 mm. (b) *IV* characteristics measured for different channel lengths. (c) Resistance *vs.* channel length. The experimental data follows a linear trend and the contact resistance can be found from the crossing of the linear trend with the vertical axis.

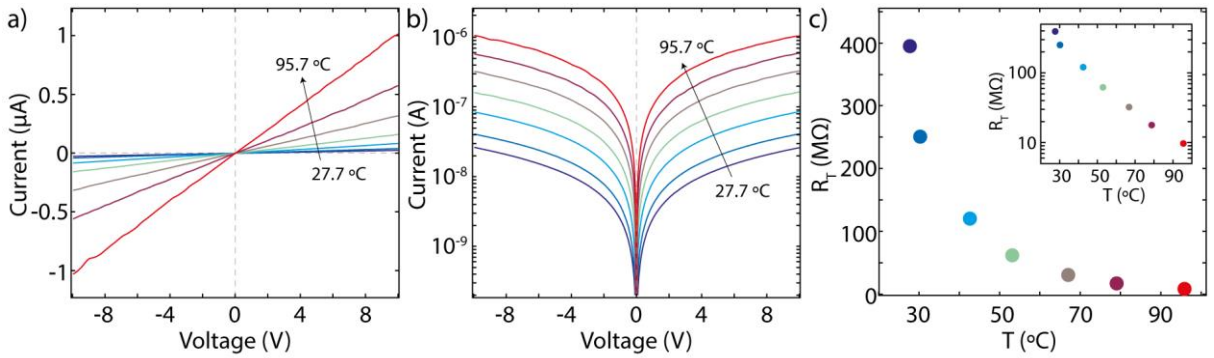

Figure S2. Temperature dependent electrical characteristics. (a) *IV* characteristics of a MoS_2 photodetector device acquired at different temperatures. (b) Absolute value of the current (in logarithmic scale) *vs.* bias voltage at different temperatures. This representation allows to better resolve the electrical characteristics changes upon heating. (c) Resistance as a function of the temperature. (Inset in c) semilogarithmic plot of the temperature dependence of the resistance where the exponential decay of the resistance with temperature is evident.

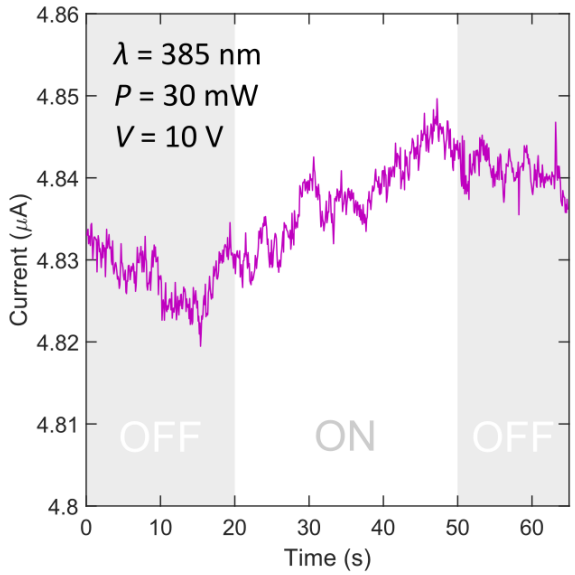

Figure S3. Current flowing across a graphite-on-paper device (similar to that shown in Figure 1 but with graphite channel instead of MoS_2), at a fixed bias voltage V = 10V, as a function of time while a 385 nm illumination source is switched ON and OFF. The graphite channel has been fabricated by rubbing graphite powder with a cotton swab.

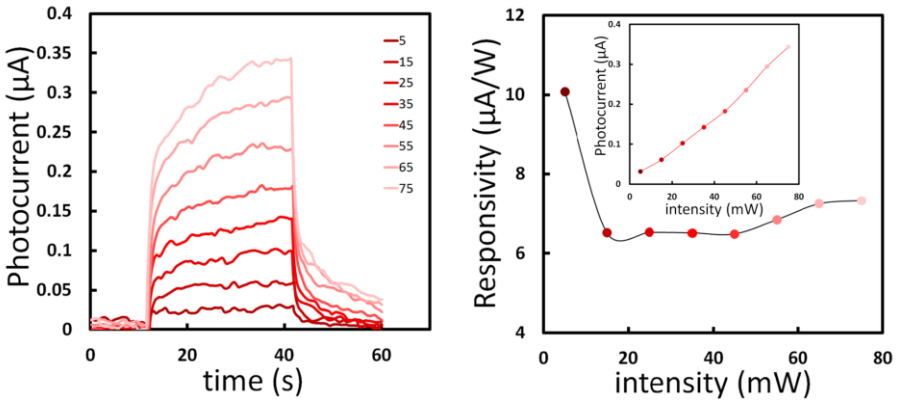

Figure S4. Photoresponse measured at 70 ºC. (left) Power dependence of the photocurrent (at a fixed bias voltage V = 20 V, wavelength λ = 660 nm and temperature T = 70 ºC). (right) Responsivity as a function of the incident power showing a rather constant value around 7 μA/W. (inset) Photocurrent *vs*. incident power relationship.